








RESEARCH ARTICLE

Structural basis for binding of the renal carcinoma target hypoxia-inducible factor 2 α to prolyl hydroxylase domain 2

William D. Figg, Jr.¹  | Giorgia Fiorini¹  | Rasheduzzaman Chowdhury¹  |
 Yu Nakashima^{1,2}  | Anthony Tumber¹  | Michael A. McDonough¹  |
 Christopher J. Schofield¹ 

¹Chemistry Research Laboratory, Department of Chemistry and the Ineos Oxford, Institute for Antimicrobial Research, University of Oxford, Oxford, UK

²Institute of Natural Medicine, University of Toyama, Toyama, Japan

Correspondence

Christopher J. Schofield, Chemistry Research Laboratory, Department of Chemistry and the Ineos Oxford Institute for Antimicrobial Research, University of Oxford, 12 Mansfield Rd, Oxford OX1 3TA, UK.

Email: christopher.schofield@chem.ox.ac.uk

Funding information

Wellcome Trust, Grant/Award Number: 091857/7/10/7; Biotechnology and Biological Sciences Research Council, Grant/Award Numbers: BB/R013829/1, BB/J001694/2, BB/L000121/1; Cancer Research UK, Grant/Award Number: C8717/A18245; Diamond Light Source, Grant/Award Numbers: MX-18069-86, MX-18069-63

Abstract

The hypoxia-inducible factor (HIF) prolyl-hydroxylases (human PHD1-3) catalyze prolyl hydroxylation in oxygen-dependent degradation (ODD) domains of HIF α isoforms, modifications that signal for HIF α proteasomal degradation in an oxygen-dependent manner. PHD inhibitors are used for treatment of anemia in kidney disease. Increased erythropoietin (EPO) in patients with familial/idiopathic erythrocytosis and pulmonary hypertension is associated with mutations in *EGLN1* (PHD2) and *EPAS1* (HIF2 α); a drug inhibiting HIF2 α activity is used for clear cell renal cell carcinoma (ccRCC) treatment. We report crystal structures of PHD2 complexed with the C-terminal HIF2 α -ODD in the presence of its 2-oxoglutarate cosubstrate or N-oxalylglycine inhibitor. Combined with the reported PHD2.HIF α -ODD structures and biochemical studies, the results inform on the different PHD.HIF α -ODD binding modes and the potential effects of clinically observed mutations in HIF α and PHD2 genes. They may help enable new therapeutic avenues, including PHD isoform-selective inhibitors and sequestration of HIF2 α by the PHDs for ccRCC treatment.

KEYWORDS

Belzutifan, clear cell renal cell carcinoma, erythropoiesis, hypoxia-inducible factor isoform 2-alpha (HIF2 α or EPAS1), prolyl hydroxylase domain (PHD or EGLN), *Trichoplax adhaerens* and *Pseudomonas putida* prolyl hydroxylase domain (TaPHD and PPHD), α -ketoglutarate/2-oxoglutarate oxygenase

1 | INTRODUCTION

In humans and other animals, the hypoxia-inducible factor (HIF) transcription factors play key roles in responses to limiting O₂ availability by promoting context-dependent expression of genes working to alleviate the effects of hypoxia. HIF is an α , β -heterodimeric protein; the levels of HIF β , also known as the aryl hydrocarbon receptor nuclear translocator protein, are not regulated directly by O₂ concentrations.¹ By contrast, as a consequence of catalysis by the HIF prolyl

hydroxylase domain enzymes (human PHD1-3), HIF α levels are strongly regulated by O₂ availability.^{2,3} PHD1-3 catalyze *trans*-4-prolyl hydroxylation of the N- and C-terminal oxygen-dependent degradation (NODD and CODD, respectively) domains in HIF1-3 α isoforms (note, HIF3 α only contains a CODD) (Figure 1A). Such prolyl hydroxylation promotes binding of HIF1-3 α to the von Hippel-Lindau protein (pVHL) ubiquitin ligase complex, so signaling for proteasomal mediated hydrolysis of HIF α isoforms (Figure 1A).⁴⁻⁷ A second HIF α hydroxylase, factor-inhibiting HIF (FIH) catalyzes the C3 hydroxylation

This is an open access article under the terms of the [Creative Commons Attribution](https://creativecommons.org/licenses/by/4.0/) License, which permits use, distribution and reproduction in any medium, provided the original work is properly cited.

© 2023 The Authors. *Proteins: Structure, Function, and Bioinformatics* published by Wiley Periodicals LLC.

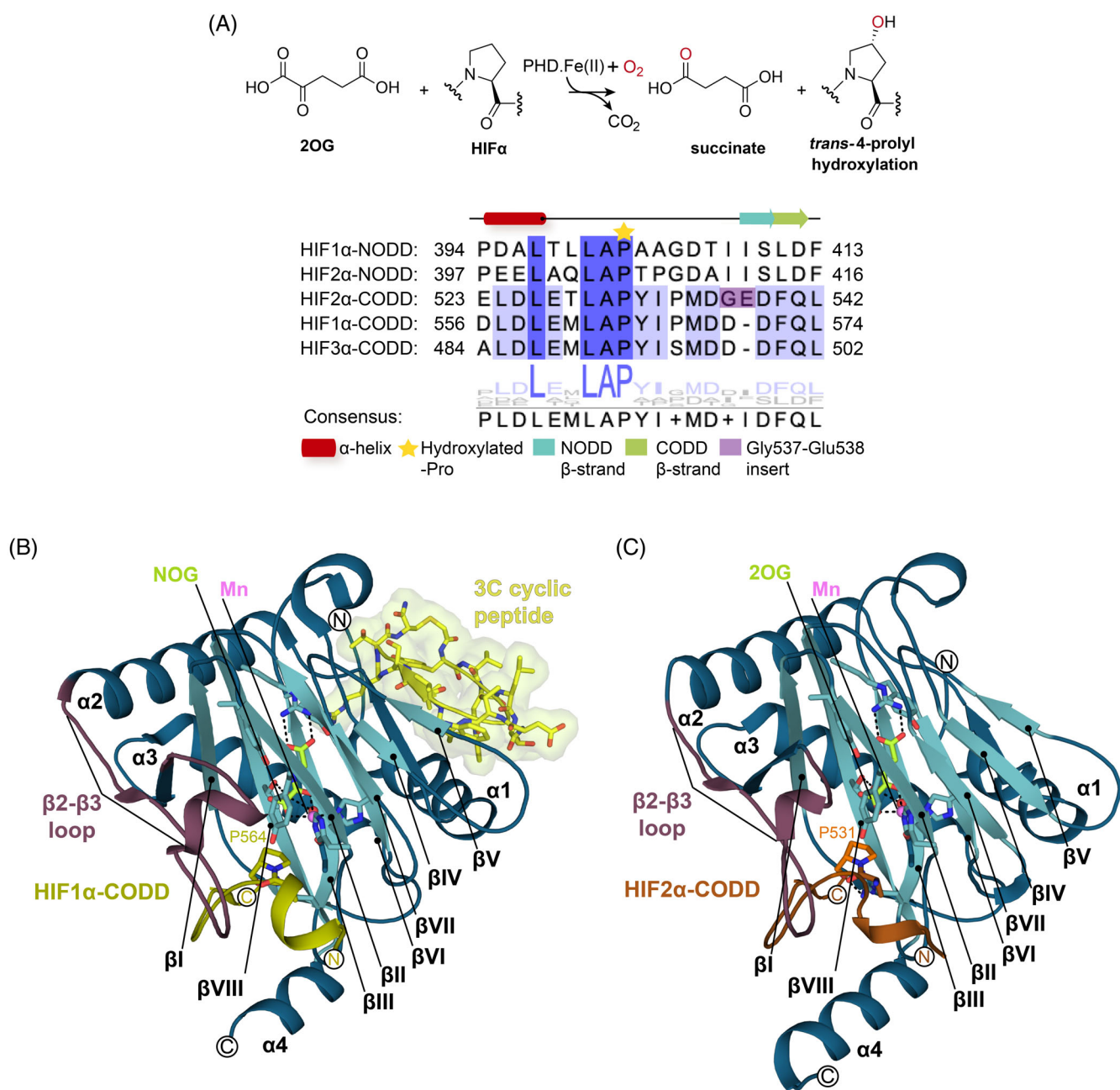


FIGURE 1 Overview of HIF α prolyl hydroxylase catalysis and view of the conserved double-stranded β -helix fold of the 2OG oxygenases. (A) PHD1-3 catalyze 2OG-dependent *trans*-4-prolyl hydroxylation of HIF α isoforms. Sequence alignment of the five human HIF α N-/C-terminal oxygen-degradation domains. The secondary structure (α -helix: red and β -strand: orange-NODD/green-CODD) assignments are as observed in crystal structures of HIF1 α ₃₉₄₋₄₁₃-NODD and HIF1 α ₅₅₆₋₅₇₄-CODD in complex with the PHD2 catalytic domain (PDB: 5L9V and 5L9B). The hydroxylated proline is marked with a yellow star. (B, C) The distorted double-stranded β -helix core fold (teal β I- β VIII refer to the eight DSBH strands), the β 2- β 3 finger loop (red cartoon), and the N-/C-terminal extensions of the DSBH (N: α 1- α 3 and C: α 4 helices-blue) are labeled. (B) The PHD2₁₈₁₋₄₀₇.Mn(II).NOG.HIF1 α -CODD.3C (6YW3) complex is depicted as a cartoon showing the N-terminal binding site of the co-crystallized 3C cyclic peptide (yellow sticks with Connolly surface). (C) A view of the DSBH of the PHD2₁₈₁₋₄₀₇.Mn(II).2OG.HIF2 α -CODD (7Q5X) complex, the main focus of this work. Key active site residues (teal), target proline (orange), and NOG (lemon) are represented as sticks. The HIF1 α -CODD (olive) and HIF2 α -CODD (orange) substrates are displayed as cartoons. Waters (red) and Mn (violet) are shown as spheres. CODD, C-terminal oxygen-dependent degradation; HIF, hypoxia-inducible factor; NODD, N-terminal oxygen-dependent degradation.

of an asparagine-residue in the C-terminal transcriptional activation domains of HIF1 α and HIF2 α (but not HIF3 α), a modification that reduces the interaction of HIF with histone acetyltransferases (CREB binding protein and p300).⁸ The FIH catalyzed modification inhibits

HIF-mediated transcription in an incompletely understood context-dependent manner (Figure S1).⁸⁻¹¹

In hypoxia, PHD1-3 activity decreases and HIF1-3 α levels rise (Figure S1).^{2,3} HIF1-3 α translocate to the nucleus and dimerize with

HIF β to form transcriptionally active α,β -HIF heterodimers (Figure S1).^{2,3,12} These bind to hypoxia response elements (HREs) associated with HIF target genes and consequently upregulate transcription of HIF controlled genes including those encoding for erythropoietin (EPO) and vascular endothelial growth factor (VEGF) (Figure S1).^{1-3,13}

The PHDs and FIH are both Fe(II) and 2-oxoglutarate (2OG)-dependent oxygenases that couple hydroxylation with the conversion of 2OG to succinate and CO₂ (Figures 1A and S1).^{3,8,11,14,15} Other human 2OG oxygenases have roles in the regulation of gene expression (e.g., the JmjC histone demethylases), and in other important cellular processes, including metabolism and collagen biosynthesis.^{14,16-18} The biochemical properties of the PHDs are apparently suited to their roles as hypoxia/"O₂-sensors"; thus, they have unusually high K_m values for O₂ and react relatively slowly with O₂, compared to FIH and most other 2OG oxygenases.¹⁹⁻²² PHD2 also forms a relatively stable complex with Fe and 2OG, even after exposure to O₂. Collectively, these observations suggest that the biochemical properties of the PHDs may be focused to sense O₂ availability.¹⁹⁻²³ The PHDs are more sensitive than FIH to limiting O₂ levels²⁴ and HIF α -NODD hydroxylation is reported to be more sensitive than CODD hydroxylation to O₂ levels.^{24,25} The PHDs also show different selectivity toward the various HIF α -ODDs, with PHD3 being reported to be particularly selective for the HIF1 α - and HIF2 α -CODD domains (Figures 1A and S1).^{12,22,26}

Crystal structures of PHD2.HIF α -ODD complexes and kinetic studies have revealed the importance of a conformationally mobile loop (the β 2- β 3 loop) that links β 2 and β 3 of the catalytic domain of PHD2 and which is involved in HIF α -ODD binding and selectivity; in the PHD2 substrate complexes, the β 2- β 3 loop folds to isolate the HIF α -ODD substrate proline at the active site.^{11,27-30} Overall, these observations support the proposal that β 2- β 3 loop dynamics are important both in catalysis and determining PHD/HIF α -ODD substrate selectivity, though the precise molecular details are undefined (Figure 1B,C).^{27,29,30}

VHL gene mutation is common in clear cell renal cell carcinoma (ccRCC) patients causing upregulation of HIF α isoforms, so increasing the expression of the HIF2 α target VEGF, in a manner apparently promoting tumorigenesis and cancer progression.^{31,32} Belzutifan (MK-6482 or PT-2977) inhibits HIF2 α -mediated expression and is used for ccRCC treatment (Figure S1).³³ Mutations in EPAS1 (encoding for HIF2 α), EGLN1 (encoding for PHD2), are also linked to disease, including familial/idiopathic erythrocytosis and ccRCC (Figure S2A).³⁴ Thus, structural information of how the PHDs bind HIF α -ODDs, and in particular HIF2 α , may inform on the clinically observed pathologies of the mutant EPAS1-related diseases.

Although structures of HIF1 α -CODD and NODD in complex with the catalytic domain of PHD2 are available, analogous structures with HIF2 α -CODD have not been reported.^{11,27,28} The PHD.HIF2 α -CODD complexes are of particular interest because of the disease relevance of HIF2 α and because of differences with HIF1 α /2 α -NODD and HIF1 α /3 α -CODD. In particular, HIF2 α contains an 'additional' (Gly) residue on the C-terminal side of the hydroxylated proline, compared to HIF1 α /3 α -CODD and HIF1-2 α -NODD (Figure 1A). In the respective position in HIF1/2 α -NODD,

the polar Gly537/Glu538 unit in HIF2 α is substituted by two non-polar Ile-residues (Figure 1A).

Here, we report high-resolution crystal structures of the truncated catalytic domain of PHD2 (residues 181-407) in complex with HIF2 α -CODD (residues 523-542), a manganese ion, and 2OG or its close isostere N-oxalylglycine (NOG) (Figures 1C and 2). The structures inform on differences in HIF α -ODD binding that may influence the different selectivity of the PHDs.

2 | RESULTS

2.1 | Crystallization and structural determination of the PHD2₁₈₁₋₄₀₇.HIF2 α ₅₂₃₋₅₄₂ complex

Recently, application of the random non-standard Peptide Integrated Discovery (RaPID) platform has enabled the identification of a cyclic peptide (3C) that binds tightly to PHD2 in a non-substrate competing manner.^{28,35} 3C binds to the N-terminal region of the PHD2₁₈₁₋₄₂₆ catalytic domain (residues 185-214) and promotes crystallization of the PHD2₁₈₁₋₄₂₆.HIF1 α -CODD complex (P2₁2₁2 space group; PDB: 6YW3).²⁸ We added 3C (Figures 1B and S3B) with the aim of promoting crystallization of the PHD2₁₈₁₋₄₀₇.Mn.NOg.HIF2 α -CODD complex (Table S1). A 1 mm x 100 μ m x 80 μ m plate morphology crystal (P2₁2₁2 space group) was obtained within 1 week that diffracted to 1.11 Å resolution at a synchrotron source (refined to 1.17 Å resolution) (PDB: 7Q5V) (Figure 2A and Table 1). These conditions also gave crystals of the analogous PHD2₁₈₁₋₄₀₇.Mn.2OG.HIF2 α -CODD complex (P2₁2₁2 space group) that diffracted to 1.19 Å resolution (refined to 1.21 Å resolution) (PDB: 7Q5X) (Figure 2B and Table 1). Although addition of the 3C promoted crystallization of the PHD2₁₈₁₋₄₀₇.HIF2 α -CODD complexes, clear electron density for 3C was not observed in the crystal structures (Figure S3B), that is there was insufficient electron density to model in 3C as reported in the PHD2₁₈₁₋₄₂₆.HIF1 α -CODD complex structure (PDB: 6YW3).

Comparison of the overall PHD2_{181-426/407}.Mn.NOg/2OG.HIF2 α -CODD structures reveals conservation of the distorted double stranded β -helix (DSBH) and associated HIF α -ODD substrate binding elements (Figures 1B,C and 3).^{11,27,28,36,37} The NOg and 2OG structures are very similar to each other (backbone RMSD: 0.078 Å) and, to a somewhat lesser extent in terms of details, with other PHD2.HIF α -ODD structures (Figure 3).^{11,27,28} In particular, variations in the conformations of α 1, the β 2- β 3 loop, and the C-terminal α 4 regions are observed. Note that the constructs used vary in the length of their C-terminus and in our case reversible binding of 3C may promote formation of, or stabilize, specific conformations that promote crystallization (Figure 3).²⁸

The previously reported PHD2 active site chemistry is also conserved in the PHD2₁₈₁₋₄₀₇.Mn.NOg/2OG.HIF2 α -CODD structures (Figure 3),³⁷ with a single manganese ion (substituting for iron) being coordinated by the side chains of His313, Asp315, and His374, as well as a well-defined water molecule/hydroxide ion.^{11,27,28} The use of Mn(II) in PHD2 crystallization/inhibition is of interest given links between disease associated with Mn metabolism and

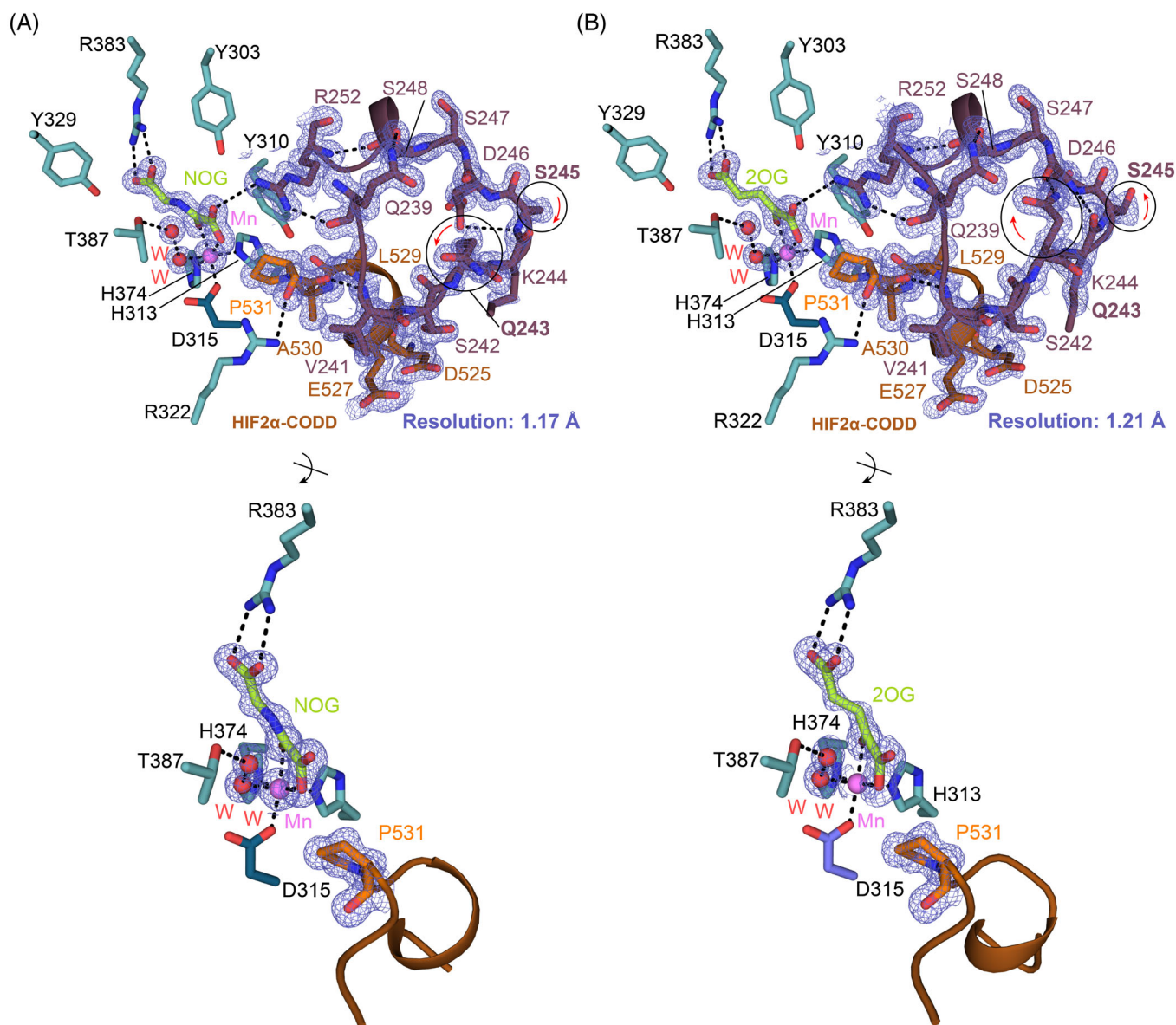


FIGURE 2 Structural basis for HIF2 α -CODD binding to PHD2. (A, B) Views from structures of PHD2₁₈₁₋₄₀₇-Mn.2OG/NOG.HIF2 α ₅₂₃₋₅₄₂-CODD displayed as cartoons (PHD2₁₈₁₋₄₀₇-blue; HIF2 α -orange) (PDB: 7Q5V-A and 7Q5X-B). PHD2 residues (blue/teal), β 2- β 3 loop (red), 2OG/NOG (lime), and HIF2 α (orange) residues are shown as sticks. The electron density map (contoured at 1.0 σ) is depicted as a mesh (blue). Key polar interactions are represented by black dashes. Waters (red) and Mn (violet) are displayed as spheres. Differences in the β 2- β 3 loop conformation in the two structures are highlighted by a black circle and a red arrow. Note the C4-*endo* conformation of the substrate proline ring in both structures. CODD, C-terminal oxygen-dependent degradation; HIF, hypoxia-inducible factor.

erythropoiesis.³⁸ 2OG and NOG bind the manganese ion in a bidentate manner via their C1 carboxylate and C2 carboxylate oxygens. The 2OG and NOG C5 carboxylates are positioned to interact with the guanidino group of Arg383 (Figures 2 and 3). The 2OG C1 carboxylate coordinates the manganese ion in the position adjacent to Pro531_{HIF2 α} , i.e., 2OG coordination is in an off-line mode, suggesting that at some stage a metal-centered rearrangement may be required to present the reactive ferryl adjacent to the oxidized Pro531_{HIF2 α} C-H bond. The pyrrolidine ring of Pro531_{HIF2 α} is clearly observed in the C4-*endo* conformation, as observed in previous PHD2-substrate complex structures.^{11,27,39} However, the C4 of Pro564_{HIF1 α} -CODD is

~ 0.5 Å closer to the metal than the Pro531_{HIF2 α} -CODD, though whether this has any kinetic relevance is unclear (Figure 3A).¹¹

Collectively, these observations reveal a conserved mode of binding for HIF α -ODD substrate proline-residues at the active site, including with respect to the substrate proline-ring conformation and off-line 2OG binding. The overall binding mode is also conserved in PHD type prolyl hydroxylases in *Trichoplax adhaerens* (TaPHD),⁴⁰ including bacteria (*Pseudomonas putida* PHD (PPHD) and *Bacillus anthracis* prolyl-4-hydroxylase (BaP4H)), which catalyze prolyl hydroxylation of elongation factor-thermally unstable (EF-Tu) (Figure S4).^{41,42} This conservation is important because these features

TABLE 1 Data collection and crystallographic processing statistics of the PHD2₁₈₁₋₄₀₇.HIF2 α complex structures.

	PHD2 ₁₈₁₋₄₀₇ .Mn(II).NOG.HIF2 α (PDB:7Q5V)	PHD2 ₁₈₁₋₄₀₇ .Mn(II).2OG.HIF2 α (PDB:7Q5X)
Beamline	Diamond Light Source-I24	Diamond Light Source-I24
Detector	Dectris Pilatus3 6M	Dectris Pilatus3 6M
Data processing	Xia2 DIALS	Xia2 DIALS
Wavelength (Å)	0.96861	0.97962
Resolution range (Å)	43.64–1.17 (1.21–1.17)	43.48–1.21 (1.25–1.21)
Space group	<i>P</i> 2 ₁ 2 ₁ 2	<i>P</i> 2 ₁ 2 ₁ 2
Unit cell (Å)	130.91 38.32 42.88	130.45 38.17 42.75
Total reflections	1 764 477 (121 954)	808 554 (71 010)
Unique reflections	73 707 (7148)	66 188 (6526)
Multiplicity	23.9 (15.4)	12.2 (10.4)
Completeness (%)	99.75 (98.07)	99.94 (99.85)
Mean I/sigma(I)	11.13 (1.20)	10.05 (1.15)
Wilson B-factor (Å ²)	13.75	14.13
R-merge ^a	0.1467 (3.871)	0.1317 (4.204)
R-meas	0.1499 (3.99)	0.1376 (4.413)
R-pim	0.03046 (0.9422)	0.03926 (1.322)
CC1/2	0.999 (0.39)	0.999 (0.432)
CC*	1 (0.749)	1 (0.777)
Reflections used in refinement	73654 (7115)	66197 (6516)
Reflections used for R-free	3747 (345)	3329 (334)
R-work ^b	0.1570 (0.3095)	0.1570 (0.3118)
R-free ^b	0.1792 (0.3188)	0.1759 (0.3075)
CC (work)	0.975 (0.722)	0.973 (0.775)
CC (free)	0.961 (0.705)	0.961 (0.805)
Number of non-hydrogen atoms	2416	2269
Macromolecules	2105	2036
2OG/NOG	13	14
Formic acid	12	44
Cl ion	1	3
Mg ion	3	3
PEG	51	17
Glycerol	13	13
Mn ion	1	1
Solvent	277	159
Protein residues	243	240
RMS (bonds, Å)	0.008	0.011
RMS (angles, °)	1.02	1.22
Ramachandran favored (%)	97.91	97.88
Ramachandran allowed (%)	2.09	2.12
Ramachandran outliers (%)	0.00	0.00
Rotamer outliers (%)	1.37	1.43
Clashscore	5.94	4.63
Average B-factor (Å ²)	23.66	23.02
Macromolecules	18.5	20.92
2OG/NOG	15.65	18.676
Formic acid	56.16	39.33

TABLE 1 (Continued)

	PHD2 ₁₈₁₋₄₀₇ .Mn(II).NOG.HIF2 α (PDB:7Q5V)	PHD2 ₁₈₁₋₄₀₇ .Mn(II).2OG.HIF2 α (PDB:7Q5X)
Cl ion	80.79	58.14
Mg ion	45.82	46.61
PEG	52.52	49.65
Glycerol	74.27	58.14
Mn ion	9.30	9.85
Solvent	32.16	33.86
Number of TLS groups	9	10

Note: Single crystal diffraction data were collected from samples at 100K with conventional, rotation-based methods. Statistics for the highest-resolution shell are in parentheses. R_{factor} is equal to $\sum_{hkl} |F_{\text{obs}}(hkl) - F_{\text{calc}}(hkl)| / \sum_{hkl} |F_{\text{obs}}(hkl)|$ and was calculated for the working set of reflections (R_{work}). R -merge (or R_{sym}) is equal to $\sum |I - \langle I \rangle| / \sum I$. R -merge represents the data quality of merged reflection data. I is equal to the intensity of individual measurements and $\langle I \rangle$ is equal to the average of multiple measurements.

R_{free} is the R_{factor} for 5% of the reflections which were excluded during refinement.

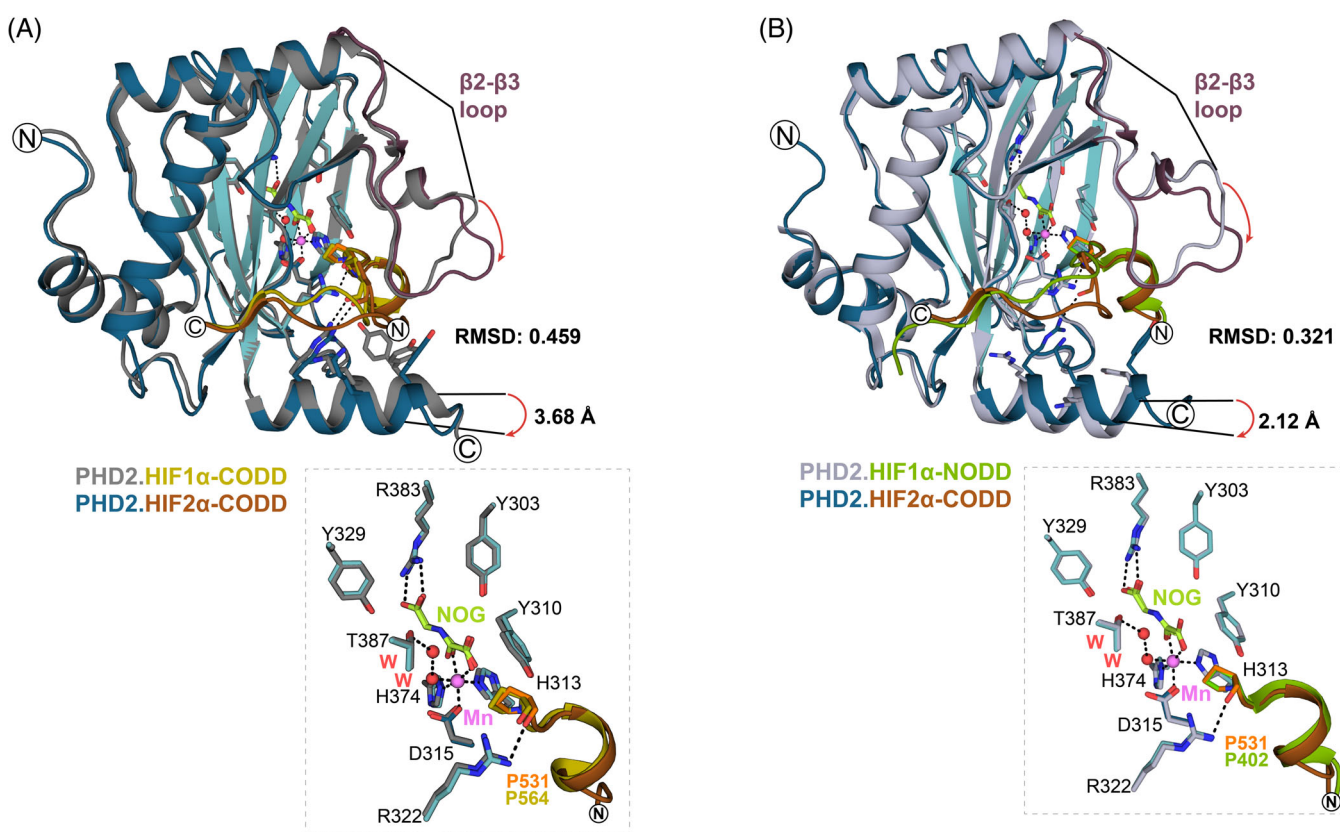


FIGURE 3 Comparison of crystal structure views of PHD2.NOG.HIF1 α -NODD/CODD complexes. (A, B) Views from structures of PHD2 (light blue-5L9V, gray-3HQR, and blue/cyan-7Q5V) complexed with HIF1 α ₃₉₄₋₄₁₃-NODD (green-5L9V), HIF1 α ₅₅₆₋₅₆₄-CODD (olive-3HQR), and HIF2 α ₅₂₃₋₅₄₂-CODD (orange-7Q5V). Polar interactions are represented by dashes (black). Waters (red) and Mn (violet) are displayed as spheres. RMSD values for aligned PHD2.HIF1 α -NODD/CODD complexes were calculated using PyMOL™. Variations in the β 2- β 3 loop and α 4-helix conformations are highlighted with red arrows. (A) Comparison of PHD2₁₈₁₋₄₂₆.NOG.HIF1 α -CODD (3HQR) and PHD2₁₈₁₋₄₀₇.NOG.HIF2 α -CODD (7Q5V) structures with a view of the active site residues and target prolines. (B) Comparison of PHD2₁₈₁₋₄₂₆.NOG.HIF1 α -NODD (5L9V) and PHD2₁₈₁₋₄₀₇.NOG.HIF2 α -CODD (7Q5V) structures with view of the active site residues and target prolines. CODD, C-terminal oxygen-dependent degradation; HIF, hypoxia-inducible factor; NODD, N-terminal oxygen-dependent degradation.

are proposed to be involved in the HIF/PHD/VHL “O₂-sensing” mechanism. Thus, off-line 2OG binding may help enable the slow reaction of the PHDs with O₂, a property proposed to be important in their “O₂-sensing” role.⁴³ C4 proline hydroxylation is proposed to enable a stereoelectronic preference for the C4-*exo* over the C4-*endo*

proline ring conformation, with the former being observed in PHD. HIF α -ODD complexes and the latter in VHL.hydroxylated-HIF α -ODD complexes.^{11,39,44}

Comparison of reported PHD2₁₈₁₋₄₂₆.NOG.HIF1 α -ODD complex structures (PDB: 3HQR and 5L9V) with the new PHD2₁₈₁₋₄₀₇.NOG.

HIF2 α -CODD (PDB: 7Q5V) structure reveals a shift in the position of the C-terminal α 4-helix relative to the core DSBH fold, which is manifested in differences in the positions of PHD2 Thr405 and Lys402 as observed in overlaid structures. Analysis of the Thr405 C α positions reveals a shift of ~ 3.7 Å in the new PHD2₁₈₁₋₄₀₇-HIF2 α -CODD complex structure (PDB: 7Q5V) compared to the PHD2₁₈₁₋₄₂₆-HIF1 α -CODD complex structure (PDB: 3HQR). Comparison of the PHD2₁₈₁₋₄₀₇-HIF2 α -CODD structure (PDB: 7Q5V) with the PHD2₁₈₁₋₄₂₆-HIF1 α -NODD structure (PDB: 5L9V) reveals a shift of ~ 2.1 Å for the Lys402 C α (Figure 3). These differences in α 4 might, in part, reflect variations in the HIF α -ODD substrate binding modes at the C-terminal region of PHD2 and their impact on catalysis.^{27,29,30} However, it cannot be ruled out if these are caused by variations in crystal lattice packing, possibly relating to 3C binding.²⁸

The β 2- β 3 loops of the PHDs are important in catalysis and in determining HIF α -ODD substrate selectivity.^{27,30,37} In the absence of HIF α -ODD substrates, the β 2- β 3 loop is likely conformationally mobile/disordered and principally adopts conformations that are not near the active site, including those observed by crystallography.^{11,27-29,45} In all reported PHD2.HIF α -ODD structures, the β 2- β 3 loop folds to enclose the substrate proline residue in the active site, as is observed in our PHD2₁₈₁₋₄₀₇-HIF2 α -CODD structures (Figure 2).

Although the overall PHD2₁₈₁₋₄₀₇-HIF2 α -CODD structures with NOG and 2OG are very similar (RMSD: 0.078 Å), there are some differences in the conformations of the β 2- β 3 loop involving PHD2 residues Gln243-Asp246 (Figure 2). In the 2OG.HIF2 α -CODD complex, the side chain amide NH₂ group of PHD2 Gln243 _{β 2- β 3} is positioned to form a hydrogen bond (2.74 Å) with the main chain carbonyl O atom of PHD2 Asp246 (Figure 2B). This hydrogen bond is, however, not observed in the NOG.HIF2 α -CODD complex, where Gln243 _{β 2- β 3} is oriented away from the loop and adopts a more solvent-exposed position (Figure 2A).

Although further work is required, given the 2OG and isosteric NOG structures have the same space group and similar crystal packing, the differences in the β 2- β 3 loop between them suggests that small differences at the active site region may influence the conformation of relatively distant structural elements within PHD2₁₈₁₋₄₀₇. This observation is interesting in part because recent studies on the mechanism of isopenicillin N synthase, which is structurally and mechanistically related to the 2OG-dependent oxygenases, imply that conformational changes distant from the active site are involved in catalysis.⁴⁶ It is also of interest because it supports the previous proposal that inhibition by 2OG mimetics involves effects on structural dynamics in addition to simple blockade of 2OG binding in the active site.^{30,47,48} Modeling studies on 2OG oxygenases, including demethylases, also imply the relevance of conformational changes both at and relatively distant from the active site during catalysis.^{49,50} However, defining the precise effects of Fe-binding inhibitors on the overall structural dynamics (and in some cases including complexed substrate) is technically challenging, requiring room temperature solution as well as low-temperature biophysical crystallographic studies.⁴⁸ Hence, in addition to studies with isolated PHDs, empirical optimization of inhibitors in a cellular context is desirable.

We compared the β 2- β 3 loop conformations in PHD2₁₈₁₋₄₀₇-2OG/NOG.HIF2 α -CODD with those of the other PHD2.HIF α -ODD complexes. An intra-loop Gln243 hydrogen bond with the main chain carbonyl O of Asp246 is observed in the PHD2₁₈₁₋₄₂₆-NOG.HIF1 α -NODD (PDB: 5L9V), PHD2₁₈₁₋₄₂₆-2OG.HIF1 α -CODD (PDB: 5L9B), and our PHD2₁₈₁₋₄₀₇-2OG.HIF2 α -CODD complexes.²⁷ In the case of the PHD2₁₈₁₋₄₂₆-NOG.HIF1 α -CODD (PDB: 3HQR)¹¹ and PHD2₁₈₁₋₄₀₇-NOG.HIF1 α -CODD.3C (PDB: 6YW3)²⁸ complexes, the side chain of Gln243 is not involved in hydrogen bonding; instead, Gln243 is in a more solvent-exposed conformation, as observed in our PHD2.NOG.HIF2 α -CODD structure (similarly, the side chain of Ser245 adopts a different conformation in the 2OG complexed structure (PDB: 7Q5X)) when compared to the NOG complex (PDB: 7Q5V) (Figure 2). Although these crystallographic observations likely reflect snapshots of β 2- β 3 loop conformations in solution, they further highlight the importance of the mobility of the β 2- β 3 loop in catalysis.

Binding of the residues to the N-terminal side of the substrate proline residue in the structures of PHD2 in complex with HIF1 α ₅₅₆₋₅₇₄.CODD and HIF1 α ₃₉₄₋₄₁₃.NODD involves interactions with β II, β II/III loop, β 2- β 3 loop, β III, β VI-VII, and β VIII (β I- β VIII refer to the eight β -strands of the DSBH).^{27,36,37} Binding of the residues to the C-terminal side of the substrate proline residues of these peptides involves interactions with β VIII, β III, helix α 3, and the α 3- β I loop. Notably, the structures show that the CODD substrates are observed to make more polar and hydrophobic interactions with the C-terminal α 4 compared to HIF1 α -NODD (Lys400_{PHD2}-Asp571_{HIF1 α -CODD}/Asp538_{HIF2 α -CODD}; Tyr403_{PHD2}-Asp536_{HIF2 α -CODD}; Tyr403_{PHD2}-Met568_{HIF1 α -CODD}/Met535_{HIF2 α -CODD}), though the mobile C-terminal region is likely involved in catalysis in all cases.^{11,27} Notably, residues Val241, Ser242, Lys244, and Ile251 of the β 2- β 3 loop interact with Glu560/Met561_{HIF1 α -CODD} and Thr398/Leu399_{HIF1 α -NODD}, via interactions with the "XX" residues of the conserved LXXLAP motif present in all HIF α -ODDs, highlighting the role of the β 2- β 3 loop in productive positioning of the different HIF α -ODD substrates (Figure 4A,B).^{11,27}

In our PHD2₁₈₁₋₄₀₇-HIF2 α ₅₂₃₋₅₄₂-CODD structures, interactions of the HIF α -ODD residues with residues both on the N-terminal and C-terminal sides of the target proline peptide with PHD2 are conserved, including the interaction with α 4 (Arg396_{PHD2}-Asp539_{HIF2 α -CODD}) (Figure 4C). The β 2- β 3 loop residues (Val241, Ser242, Lys244, and Ile251) interact with Glu527/Thr528_{HIF2 α -CODD} ("XX" residues of the LXXLAP motif of HIF2 α -CODD) in a similar fashion to the previously reported PHD2 structures with HIF1 α -NODD/-CODD.²⁷

These combined observations further support a role for the β 2- β 3 loop in positioning the HIF α -ODD substrates at the PHD active site, notably via interactions with the conserved LXXLAP motif in HIF α -ODDs. Despite most of the interactions appearing to be conserved in the different HIF α -ODDs, a striking conformational feature is observed at the C-terminal site of HIF2 α ₅₂₃₋₅₄₂-CODD in both the 2OG and NOG PHD2₁₈₁₋₄₀₇-HIF2 α -CODD complex structures (PDB: 7Q5V and 7Q5X). Glu538_{HIF2 α -CODD} is observed to adopt two conformations in both structures, one of which, conformation-A, is less solvent exposed and one of which, conformation-B, is more solvent

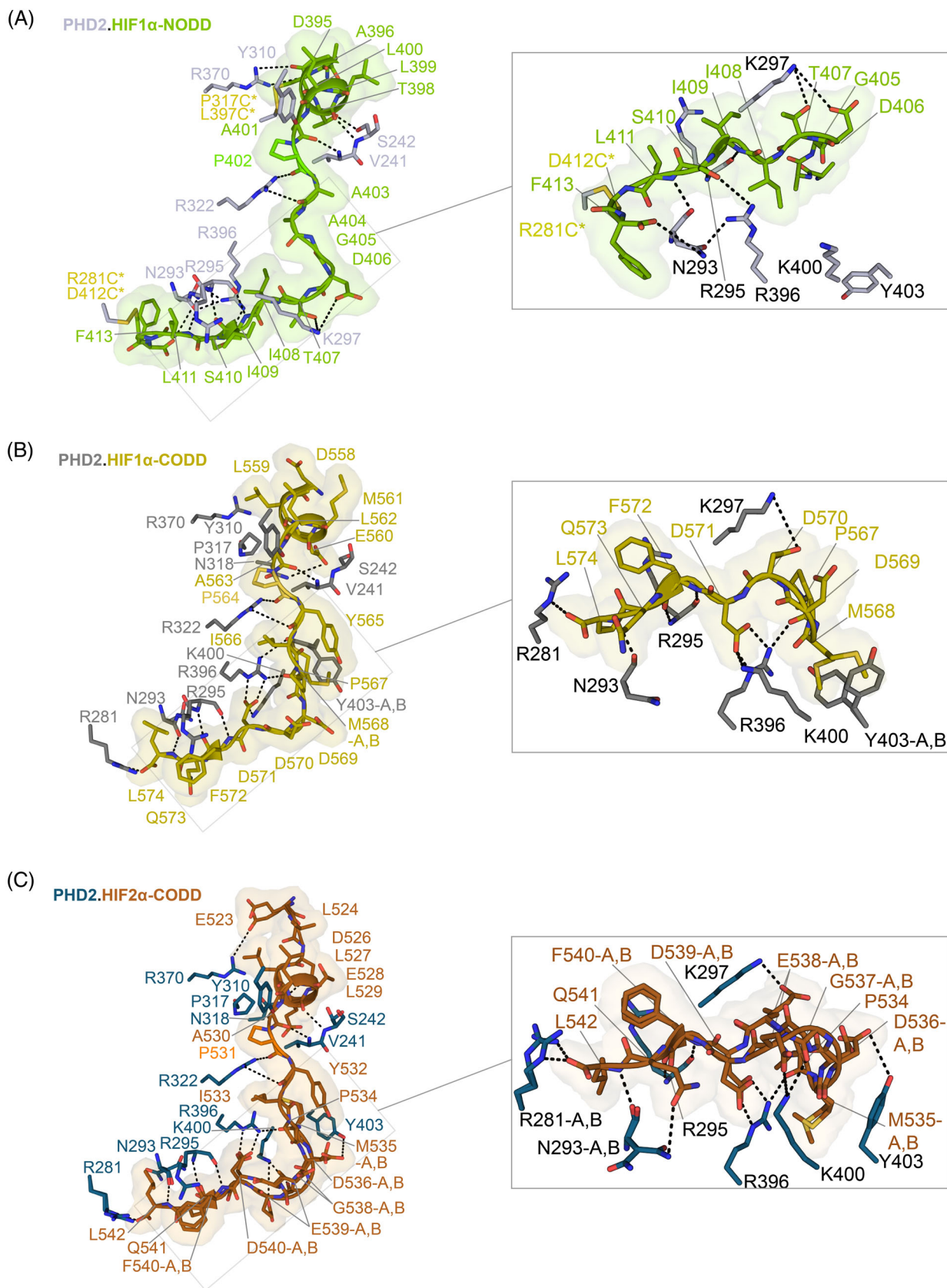


FIGURE 4 Comparison of PHD2.HIF α -ODD binding interactions. (A–C) Views showing the conformations of HIF1-2 α (HIF1 α -NODD-green, HIF1 α -CODD-olive, and HIF2 α -CODD-orange) as observed by crystallography in complex with truncated PHD2 displayed as sticks with solvent-excluded surface representation (Connolly) (PDB: 5L9V-gray, 7Q5V-blue, and 3HQR-dark gray). HIF1-2 α -ODDs are displayed as cartoons and sticks. Hydrogen bonding and electrostatic interactions are represented by black dashes. (A) Disulfide cross-linked residues in (A), produced to enable stable complex formation, are shown as yellow sticks. CODD, C-terminal oxygen-dependent degradation; HIF, hypoxia-inducible factor; NODD, N-terminal oxygen-dependent degradation.

exposed. In conformation-B, Glu538_{HIF2 α -C-ODD} projects towards a symmetry-related chain forming a hydrogen bond with Glu538_{HIF2 α -C-ODD} in a symmetry-related molecule (Figure S3A). It is possible that the conformational flexibility of Gly537_{HIF2 α }/Glu538_{HIF2 α }} unit relates to the presence of the additional Gly537 in HIF2 α -C-ODD on the C-terminal side of the hydroxylated proline, compared to HIF1 α /3 α -C-ODD and HIF1/2 α -NODD (Figure 1A). When compared with HIF1/2 α -NODD, hydrophobic Ile-residues are in the same position as the polar Gly/Glu unit of HIF2 α -C-ODD; these may alter the dynamics of the enzyme-substrate interaction (Figure 1A).²⁷}

The above-described differences may, at least to some extent, influence PHD2 HIF α -isoform selectivity. To investigate the preference of PHD2 towards HIF α -C-ODD substrates, we carried out assays comparing the PHD2 catalyzed hydroxylation of HIF1-3 α C-ODD peptides, both individually and as a mixture (Figure 5). The results with PHD2 and individual peptides showed no clear preference for the

HIF1-3 α -C-ODD. However, when conducting the reaction with a 1:1:1 mixture of HIF1-3 α -C-ODD peptides, PHD2 showed a clear preference for HIF1 α - over the HIF3 α - and HIF2 α -C-ODDs (Figure 5A). This result supports the proposal that the presence of the additional Gly537/Glu538 unit in HIF2 α -C-ODD on the C-terminal side of the hydroxylated proline, compared to HIF1 α /3 α -C-ODD causes PHD2 to preferentially catalyze hydroxylation of HIF1 α peptide over HIF2-3 α -C-ODDs peptides.⁵¹ The Gly537/Glu538 unit in HIF2 α -C-ODD may also reflect differences in crystallization conditions required for the various PHD2.HIF α -ODD complexes (Table S1).

2.2 | Structural comparison of PHD1-3.HIF1-3 α between crystallographic and AlphaFold predicted structures

Although structures of PHD2 in complex with HIF1-2 α -C-ODD and HIF1 α -NODD are available,^{11,27,52} analogous structures of PHD1 and PHD3 complexed with HIF α -ODDs are not reported. To gain insight into how structural differences between PHDs may influence isoform selectivity toward HIF α -substrates, we built AlphaFold models⁵³ of PHD1 (UniProt: Q96KS0) and PHD3 (UniProt: Q9H6Z9) and compared these with the PHD2 crystal structures (Figures S5 and S6). The structural alignments imply variations in the conformations of residues in the DSBH β II/ β III loop and β 2- β 3 loop regions (Figures 1B,C, S5, and S6). The predicted PHD1 DSBH β II/ β III loop region differs from that of PHD2 at two residues (Lys291_{PHD2}/Val297_{PHD1} and Asn318_{PHD2}/His302_{PHD1}) and at four residues in the β 2- β 3 loop region (Ser247_{PHD2}/Pro231_{PHD1}, Ser248_{PHD2}/Pro232_{PHD1}, Asp250_{PHD2}/Ser234_{PHD1}, Asp246/Ile230_{PHD1}). The predicted PHD3 β 2- β 3 loop differs at eight residues compared with PHD2 (Gln243_{PHD2}/Ala66_{PHD3}, Leu244_{PHD2}/Arg65_{PHD3}, Ser242_{PHD2}/Pro64_{PHD3}, Arg281_{PHD2}/Leu103_{PHD3}, Asn293_{PHD2}/Lys115_{PHD3}, Lys291_{PHD2}/Tyr113_{PHD3}, Gly294_{PHD2}/Glu116_{PHD3}, Tyr403_{PHD2}/Phe225_{PHD3}) (Figure S5B).

Comparison of the binding modes of HIF α -ODDs C-terminal to the proline substrate PHD1-3 implies that most of the key protein:substrate interactions are conserved in the analogous PHD1 and PHD2 complexes (Figure S5). By contrast, although care should be taken not to over interpret the preliminary models, more apparent differences are observed between PHD3 and PHD2 (and by implication PHD1). In the PHD2_{181-426/407}-HIF1-2 α -C-ODD structures (PDB: 3HQ9 and 7Q5V), Arg281_{PHD2} interacts with residues C-terminal to the target prolines of the HIF1-2 α -C-ODD substrates, that is Leu574_{HIF1 α }} and Leu542_{HIF2 α }}, respectively. These interactions may not occur (or occur differently/less efficiently) in PHD3 where Arg281 is replaced by Leu103 (Figure S5D,E). Additionally, in the PHD2₁₈₁₋₄₂₆-HIF1 α -NODD complex structure (PDB: 5L9V), Arg396_{PHD2} is positioned to form a polar interaction with Ser410_{HIF1 α -NODD} (Figure 5B). In the PHD3 model, Ser410_{HIF1 α -NODD} is positioned to interact with Glu116_{PHD3}. Further, in the PHD3 model, the Tyr113_{PHD3} and Lys115_{PHD3} side chains clash with Phe413_{HIF1 α -NODD} (Figure S5C). The relative lack of predicted

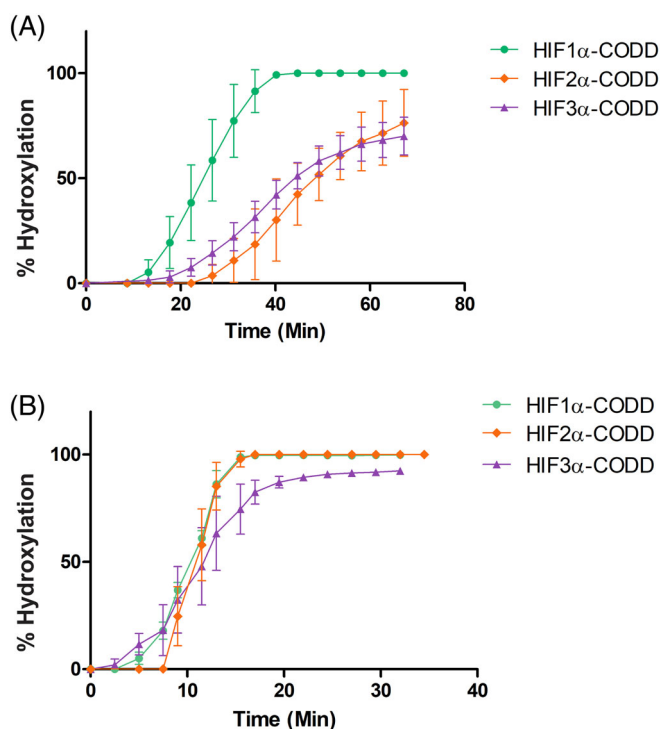


FIGURE 5 PHD2.HIF α -C-ODD hydroxylation assays. (A, B) Studies on the HIF α -C-ODD selectivity of PHD2₁₈₁₋₄₂₆. The following C-ODD peptides (with C-terminal amides) were used: HIF1 α ₅₅₆₋₅₇₄-C-ODD (DLDLEMLAPYIPMDDDFQL), HIF2 α ₅₂₃₋₅₄₂-C-ODD (ELDLETLAPYIPMDGEDFQL) and HIF3 α ₄₈₄₋₅₀₅-C-ODD (ALDLEMLAPYISMDDDFQLN). (A) 200 μ M sodium-L-ascorbate, 20 μ M 2OG, 20 μ M (NH₄)₂Fe(II)SO₄, and HIF1-3 α -C-ODD peptides (each at 10 μ M) were mixed in a ratio of 1:1 with 300 nM PHD2₁₈₁₋₄₂₆. Hydroxylation (%) was measured in real time (min) by SPE-MS-based enzymatic assays. (B) Single peptide control reaction conditions: 200 μ M sodium-L-ascorbate, 20 μ M 2OG, 20 μ M (NH₄)₂Fe(II)(SO₄), and individual HIF α -C-ODD peptides (10 μ M) with 300 nM of PHD2₁₈₁₋₄₂₆. C-ODD, C-terminal oxygen-dependent degradation; HIF, hypoxia-inducible factor; NODD, N-terminal oxygen-dependent degradation.

interactions between PHD3 and HIF1 α -NODD might, in part, rationalize the preference of PHD3 for HIF1-2 α -CODD over NODD.²⁶

Comparison of the HIF α -ODD binding modes of PHD1-3 with respect to the N-terminal sides of the target substrate prolines (Figure S6) also implies differences in the PHD.HIF α -ODD interactions between PHD1/PHD3 models and the PHD2 crystal structures. In PHD2_{181-426/407}.HIF1-2 α -CODD structures (PDB: 3HQR and 7Q5V), Asn318_{PHD2} interacts with Glu560_{HIF1 α -CODD} and Asp525/Glu527_{HIF2 α -CODD}; the Asn318_{PHD2} side chain is in different conformations in the HIF1 α - and HIF2 α -CODD structures. In the predicted PHD1 model, Asn318_{PHD2} (DSBH β II/ β III loop) is replaced by His302_{PHD1} (Figure S6), which may interact differently with the HIF1-2 α -CODDs compared to Asn318_{PHD2}. In the PHD1 model with HIF1 α -NODD, Thr398_{HIF1 α -NODD} likely forms a polar interaction with His302_{PHD1}; however, in the covalently cross-linked PHD2₁₈₁₋₄₂₆.HIF1 α -NODD complex residues Thr398_{HIF1 α -NODD} and Asn318_{PHD2} are 5.46 Å apart, which suggests a weak interaction at this position (PDB: 5L9V). Similarly, in all reported PHD2.HIF α -ODD complexes, Ser242_{PHD2} interacts with Leu397_{HIF1 α -NODD}, Glu560_{HIF1 α -CODD}, and Asp390_{HIF2 α -CODD}. In PHD3, residue Ser242_{PHD2} (β 2- β 3 loop) is substituted by Pro64_{PHD3}, the latter of which cannot make the same polar interactions (Figure S6). Pro64_{PHD3} may also alter the dynamics of the β 2- β 3 loop during catalysis compared with PHD1-2.

The predicted weaker interactions of PHD3.NODD residues both on the N- and C-terminal sides of the proline substrate residue may explain the low level of PHD3.HIF1-2 α -NODD turnover observed from these substrates.^{26,27} Due to the preliminary nature of the models and given the multitude of interactions in the PHD.HIF α -ODD complexes, to what extent these structural conformational changes/induced fit processes directly influence catalysis and PHD isoform selectivity remains unclear.

3 | DISCUSSION

Interactions between the PHDs and the HIF α -ODDs play a central role in the hypoxic response in humans and other animals. PHD-like prolyl-hydroxylases are also present in certain non-animal eukaryotes and prokaryotes, though to date these identified substrates are not HIF (like) transcription factors. In early metazoan PHD/HIF-containing organisms, there is typically only one PHD and one HIF α , as exemplified by studies on *T. adhaerens* (Figure S4).^{40,54} However, in humans and other complex HIF containing animals, there are commonly more than one PHD isoform and more than one HIF α isoform, though (typically) likely only one von Hippel-Lindau protein and one FIH.⁵⁴ There are some subsequent bioinformatic studies that have revealed multiple PHDs and HIF α -ODDs present in complex animals, at least in part, a reflection of the need for context-dependent regulation of the hypoxic response.^{54,55} This increased complexity may introduce vulnerabilities with respect to mutations enabling specific disease states including cancer, for example, by using modulation of one HIF α isoform in tumor progression whilst maintaining an ability to execute a

robust hypoxic response, with another HIF α isoform.^{31,56,57} In this regard, the link between HIF2 α upregulation in ccRCC (most commonly associated with VHL gene mutation) and diseases related to erythrocytosis is of interest.

Reduction of HIF2 α mediated expression is the mode of action of Belzutifan which is used to treat ccRCC.^{31,33} However, there is a need for new treatments for ccRCC and other diseases associated with VHL/HIF α /PHD gene mutations. Such treatments could, in principle, involve modulation of PHD.HIF α -ODD interactions, for example, by sequestering a HIF2 α -CODD in complex with PHD, possibly in a manner that signals for a non-VHL mediated protein degradation process, by using a small-molecule and/or metal ion that promotes the PHD.HIF2 α -CODD interaction. The structures presented here may help in the design of such small molecules.

Since many mutations to the catalytic domain of PHD2 and HIF2 α -ODDs have been identified,⁵⁸⁻⁶⁴ understanding how these impact on PHD2.HIF2 α -ODD interactions is of interest in terms of understanding the molecular basis of associated diseases (Figure S2). At least some of the observed EPAS1/HIF2 α mutations will likely impact on PHD catalysis as they involve residues that interact with the PHD2 active site as shown by our PHD2₁₈₁₋₄₀₇.NOG/2OG.HIF2 α -CODD structures (PDB: 7Q5V and 7Q5X) and inferred by models of PHD1-3.HIF α -ODD complexes (Figure S2). Strikingly, some of the clinically observed mutations (M535V, M535T, G537W, and G537R) affect the Gly537/Glu538 unit, thus likely altering PHD.HIF α -ODD binding potentially in a manner affecting catalytic efficiency and/or HIF α -ODD selectivity in a disease-relevant manner. Differences in PHD1-3.HIF1-3 α -ODD related interactions are also important in the normal hypoxic response and knowledge of them may help enable treatments including modulation of specific sets of HIF target genes.

The combined crystallographic and NMR studies, further highlight the importance of the conformationally mobile β 2- β 3 loop and the C-terminal PHD region in HIF α -ODD hydroxylation and selectivity (Figures 2 and 4).^{11,27,29,30,36,45} However, the available evidence also supports the dynamic nature of PHD.HIF α -ODD interactions, at least in certain stages of the catalytic cycle. This means that structure-based attempts to modulate PHD.HIF α -ODD interactions, for example, to alter PHD isoform selectivity, should be coupled with empirical approaches in cells (note PHD.HIF α interactions likely involve other components and regions beyond the immediate PHD catalytic domain and HIF α -ODD reactions).

The presence of an additional residue (Gly537/Glu538 unit) in HIF2 α -CODD compared to other HIF α -ODDs, likely results in increased flexibility of HIF2 α -CODD, possibly weakening its binding to PHD2 (Figure S3A). This may, at least partially, explain the preference of PHD2 for HIF1 α > HIF3 α > HIF2 α -CODDs as observed in our biochemical studies (Figure 5). However, it is important to note that multiple interactions occur between the PHDs and the HIF α -ODDs and given the dynamic nature of at least some of these interactions, it is difficult to predict the effects of individual residue changes with confidence.

By contrast, the dynamic and multivalent interaction of the PHDs with the overall HIF α -ODDs, the chemistry in the immediate active site vicinity appears to be highly conserved in the PHDs, an observation which even extends, at least substantially, to PHD-like enzymes with non-HIF α substrates (Figure S4C).^{41,42} The conservation includes with respect to the nature of Fe(II) and 2OG binding, including the positioning of the 2OG C1 carboxylate adjacent to the methylene of the proline-residue that undergoes hydroxylation, an arrangement that is likely partially responsible for the unusually slow reaction of the PHDs with O₂, though other factors also likely impact this aspect of the mechanism.⁴³ Another chemically relevant conservation is the conformation of the unhydroxylated substrate proline ring at the active site, which to date has always been observed in the C4-*endo* formation, at least in the PHD2 substrate complexes. PHD catalyzed *trans*-4-hydroxylation results in a bias of the proline ring to the C4-*exo* protein conformation, due to operation of a stereoelectronic effect, as observed in pVHL-hydroxylated-HIF α -ODD complex structures.³⁹

Comparison of AlphaFold models of PHD1 and PHD3 with PHD2.HIF1-2 α -CODD and PHD2.HIF1 α -NODD structures predict differences in the β 2- β 3 loop and C-terminal regions apparently linked to differences in the HIF α -ODDs binding modes, with overall fewer interactions between the HIF α -ODDs and PHD1/3 models compared to PHD2 (Figures S5 and S6). Testing the consequences of these differences for PHD catalysis with wild-type and clinically relevant mutated HIF α -ODDs is the subject of ongoing work.

4 | EXPERIMENTAL SECTION

4.1 | Materials

Reagents, chemicals, and solvents were from Sigma-Aldrich (Merck), Apollo Scientific, or Thermo Fisher Scientific, except where stated. The HIF1 α ₅₅₆₋₅₇₄-CODD (DLDLEMLAPYIPMDDDFQL), HIF2 α ₅₂₃₋₅₄₂-CODD (ELDLETLAPYIPMDGEDFQL), and HIF3 α ₄₈₄₋₅₀₅-CODD (ALDLEMLAPYISMDDDFQLN) and 3C cyclic (d-YVWLTDTWVLSRTC)^{28,35} peptides were from GL Biochem (prepared with a C-terminal amide). Water used for cell culture was purified using a Millipore Elix[®] 10 system (Merck Life Sciences) and autoclave sterilized (Crystal 300-RP25, Rodwell Engineering Group). Water used for buffers and molecular experiments was filtered purified by a 0.22- μ m Milli-Q filtration system (Milli-Q, Merck Life Sciences). Kanamycin (final concentration 62 mM) was prepared in water sterilized by a benchtop autoclave (LTE TouchClave II, LTE Scientific; program: 121°C and 1 Bar for 15 min) and filtered for impurities with a 0.22- μ m syringe filter (Sarstedt).

4.2 | Expression and protein purification

The PHD2₁₈₁₋₄₀₇-pET-28a(+) plasmid was expressed in *Escherichia coli* BL21(DE3) cells (New England Biolab Inc.).²⁷ Expression was induced with 0.5 mM isopropyl β -D-1-thiogalactopyranoside (IPTG)

(OD_{600 nm} 0.6–1.2) at 28°C for 3–4 h.²⁷ Cells were harvested and stored at –80°C until purification. Cells were freeze-thawed at 4°C in the lysis buffer (20 mM Tris-HCl pH 7.5 RT, 0.5 M NaCl, 5 mM imidazole, and 5% (vol/vol) glycerol).²⁷ DNaseI and ethylenediaminetetraacetic acid (EDTA)-free protease inhibitor tablet (Roche) were added. Sonication (10 min total elapsed time, 3 s on/off pulse) was used for lysis (Cole-Parmer[®]-500-Watt ultrasonic homogenizer, Cole-Parmer). Cell lysates were then centrifuged (20,000 rpm, 4°C, JA-25.50 rotor-Avanti-JHC centrifuge, Beckman Coulter); the supernatant was loaded onto a 5-mL HisTrap[™] column (GE Life Sciences) for Ni(II) affinity chromatography. A 5-mL HisTrap[™] column was charged with 5 column volumes (CVs) of 100 mM Ni(II)SO₄, then washed with 5 CV of lysis buffer, followed by 5 CV of elution buffer (20 mM Tris-HCl pH 7.5 room temperature [RT], 0.5 M NaCl, 0.5 M imidazole, and 5% [vol/vol] glycerol), finally with 5 CV of lysis buffer.³⁰ The loaded column was washed with 30 CV of wash buffer (20 mM Tris-HCl pH 7.5 RT, 0.5 M NaCl, 30 mM imidazole, and 5% [vol/vol] glycerol). Tagged PHD2₁₈₁₋₄₀₇ was eluted using a step gradient (5 CV each step) of increasing elution buffer (16% [vol/vol], 34% [vol/vol], and 100% [vol/vol]).³⁰ The purity of the protein fractions was analyzed by SDS-PAGE (>90% pure material was used). His₆-PHD2₁₈₁₋₄₀₇ fractions were concentrated to 5–6 mL volume with a concentrator (10 kDa cutoff, Amicon) at 4000 rpm and 4°C. To cleave His₆-tag 0.25 units of restriction grade thrombin (Novagen, Merck) and 1 \times thrombin cleavage buffer (10 \times stock of 200 mM Tris-HCl pH 8.4, 1.5 M NaCl, and 25 mM CaCl₂, Novagen, Merck) were added to tagged PHD2₁₈₁₋₄₀₇. The cleaved PHD2₁₈₁₋₄₀₇ was loaded onto a Superdex[®] 75 gel filtration column (GE Life Sciences) pre-equilibrated with 1 CV of 50 mM Tris-HCl pH 7.5 RT, 100 mM NaCl, and 1% (vol/vol) glycerol. Proteins were eluted with an isocratic gradient and fractions were collected and analyzed for purity by SDS-PAGE (estimated >90%).³⁰ PHD2₁₈₁₋₄₀₇ was buffer exchanged with a PD-10 desalting column (GE Life Sciences) into the final storage/crystallization buffer (50 mM Tris-HCl pH 7.5 RT, and 1% [vol/vol] glycerol).

4.3 | PHD2.HIF2 α -CODD complex preparation

Highly purified PHD2₁₈₁₋₄₀₇ via a two-column purification strategy (affinity and SEC chromatography) was used to obtain the PHD2₁₈₁₋₄₀₇.Mn(II).NOG/2OG.HIF2 α ₅₂₃₋₅₄₂-CODD complex crystals. Stocks of Mn(II) (100 mM), NOG pH 7–8 (80 mM), and 2OG disodium salt (100 mM) were prepared in deionized water (filter sterilized with 0.22 μ m Milli-Q filtration system, Merck Life Sciences). Cofactors/inhibitors were diluted to final concentrations of 1.2 mM-Mn(II) and 2 mM-NOG/2OG in the protein solution. The protein.metal.ligand mixture was pipetted directly onto lyophilized 3C cyclic peptide (weighed out at a final concentration of 2 mM into a 70- μ L final mixture volume) and left to equilibrate on a Cole-Parmer[®] tube rotator (Cole-Parmer) at 4°C for 2.5 h. PHD2₁₈₁₋₄₀₇ was centrifuged at 12000 rpm (9600g) for 10 min at 4°C. The protein (1 mM), dissolved cofactors (1.2 mM-Mn(II), 2 mM-NOG/2OG), and 3C (2 mM) mixture were added to lyophilized HIF2 α ₅₂₃₋₅₄₂-CODD peptide (weighed out for a final concentration of 2–4 mM into a 70- μ L final mixture

volume). The protein-substrate mixtures were left overnight to equilibrate on the tube rotator at 4°C. The next day, the incubated sample was centrifuged at 14,000 rpm (18,800 g) and the supernatant was harvested for crystallization. The protein-substrate sample volume was adjusted with crystallization buffer (50 mM Tris-HCl pH 7.5 RT, 1% [vol/vol] glycerol) to a final volume of 70 μ L before preparation of the crystallization plates.

4.4 | Crystallization of the PHD2₁₈₁₋₄₀₇.Mn(II).NOG/2OG.HIF2 α ₅₂₃₋₅₄₂-CODD complexes

The PHD2₁₈₁₋₄₀₇.Mn(II).NOG or 2OG.HIF2 α ₅₂₃₋₅₄₂-CODD.3C mixtures were screened against 0.25–0.39 M magnesium formate disodium salt and 18%–22% (wt/vol) poly-ethylene glycol (PEG) 3350 pH 7.0 (precipitant solutions were filtered; 0.22- μ m filter, Sarstedt).²⁸

The protein-substrate mixture was prepared with 1 mM PHD2₁₈₁₋₄₀₇, 1 mM Mn(II)Cl₂, 2 mM NOG/or 2OG, 2–4 mM HIF2 α ₅₂₃₋₅₄₂-CODD peptide, and 2 mM 3C peptide dispensed into crystallization plates (300 nL drops at 2:1 and 1:2 ratios and 200 nL drop at 1:1 ratio in Intelli-plates, Art Robbins) with a Phoenix robot (Art Robbins) at 4°C and stored at 298K. A 1 mm \times 100 μ m \times 80 μ m (PDB: 7Q5V) and a 240 μ m \times 50 μ m \times 30 μ m (PDB: 7Q5X) plate-like crystals appeared after 1-week of equilibration in 0.31 M magnesium formate and 16.6% (wt/vol) PEG 3350 (200 nL, 1:1 protein-to-well ratio, 298K). Crystals were exposed to the cryo-protectant (reservoir solution supplemented with 20% (vol/vol) glycerol), manually looped, and cryo-cooled into liquid-N₂. Crystals were stored under liquid-N₂ until data collection at the Diamond Light Source.

4.5 | Solid phase extraction-MS based enzymatic activity assays

Activity assays were conducted using a RapidFire[®] RF360 sampling robot (Agilent Technologies). Samples were loaded onto a C4 SPE cartridge (Agilent Technologies) and peptides were eluted with 85% (vol/vol) acetonitrile and 15% (vol/vol) water mixture added with 0.1% (v/v) formic acid. Real-time activity assays were performed in reaction buffer containing 50 mM Tris-HCl pH 7.8 and 50 mM NaCl. Stock solutions of each component were made freshly. 100 mM stock solution of sodium-L-ascorbate and 50 mM stock solution of 2OG were made in water (LC-MS Grade, LiChrosolv[®]). 10 mM peptides stock solution were made in dimethyl sulfoxide (DMSO). To limit oxidation of Fe(II) to Fe(III), a 100 mM stock solution of (NH₄)₂Fe(II)(SO₄) was made in HCl (20 mM), then diluted to 10 mM with water (LC-MS Grade, LiChrosolv[®]). 1 mL final volume solutions containing 200 μ M sodium-L-ascorbate, 20 μ M 2OG, 20 μ M (NH₄)₂Fe(II)(SO₄) and 10 μ M peptide (HIF1 α ₅₅₆₋₅₇₄-CODD, HIF2 α ₅₂₃₋₅₄₂-CODD, or HIF3 α ₄₈₄₋₅₀₅-CODD) were prepared as control reactions. 1 mL solutions containing 200 μ M sodium-L-ascorbate, 20 μ M 2OG, 20 μ M (NH₄)₂Fe(II)(SO₄), and 10 μ M of a 1:1:1 mixture of peptides (HIF1 α ₅₅₆₋₅₇₄-CODD, HIF2 α ₅₂₃₋₅₄₂-CODD, and HIF3 α ₄₈₄₋₅₀₅-CODD) were prepared for

the competition reactions. About 500 μ L of the substrate mixture was transferred into 96-well polypropylene plates (Agilent Technologies). After a first injection onto the C4 SPE cartridge (Agilent Technologies), data acquisition was paused, then 500 μ L of 300 nM PHD2₁₈₁₋₄₂₆ in reaction buffer was added into the well to initiate the reaction. The control reactions were monitored for 32 min (one injection every 2.5 min). The competition reactions were monitored for 67 min (one injection every 5 min). The positive ion mode was used to monitor peptide charge states. RapidFire Integrator software (Agilent Technologies) was used to integrate the area of the peaks extracted from the chromatogram. Excel was used to calculate percent (%) hydroxylation of the CODD peptide substrates using the formula: % hydroxylated substrate = 100 \times hydroxylated/(hydroxylated + non-hydroxylated peptide). Oxidation of the methionine residues in the CODD sequences was 4%–6% in the no enzyme control. Every data set was normalized to a no enzyme buffer control.

4.6 | X-ray data analysis and software

X-ray diffraction data were collected at Diamond Light Source synchrotron at I24 MX beamline and autoprocessed with Xia2 (DIALS, Diamond Light Source Ltd.).⁶⁵ PHENIX.Xtriage was used to assess the data quality of the reflections.⁶⁶ Phaser-Molecular replacement (PHASER-MR) was used to phase the processed diffraction data for the structures (PDB: 7Q5V and 7Q5X).⁶⁷ A previously determined structure of PHD2 (PDB: 3HQR) was used as a search model for MR-phasing.¹¹ COOT (version 0.9.5, CCP4) was used to semi-manual model build based on the overlaid 2mF_o-DF_c and difference mF_o-DF_c electron density maps from the phased structures (PDB: 7Q5V and 7Q5X).^{68,69} The geometry of the model was adjusted based on calculated electron density maps and was improved in COOT with subsequent refinement cycles using PHENIX.Refine.^{66,70} Three cycles were typically run for each refinement round before manual fitting. PHENIX.Refine was used to modify and improve the model in iterative cycles.⁷⁰ Model improvement was assessed by the decrease in, and convergence of R_{work}/R_{Free} values between cycles of refinement. MolProbity was used to assess the geometric quality of the refined model and to guide re-building in COOT.^{68,71} Resolution was defined depending on the completeness of the resolution bin (>95% in all resolution bins). PDB extract online tool (version 3.24, Research Collaboratory for Structural Bioinformatics PDB) was used to prepare coordinate and structure factors files in macromolecular CIF format (mmCIF) to be uploaded to Onedep for PDB deposition.⁷² PyMOL™ (Schrodinger) was used for graphical representation and structure alignment.

4.7 | Quantification and statistical analysis

GraphPad prism (version 6.0) was used to plot hydroxylation over time. Multiple sequence alignments of HIF2 α ₅₂₃₋₅₄₂-CODD (EPAS1) sequences employed ClustalOmega (EMBL-EBI) using the default settings. JalView (version 2.10.5) was used to generate figures.

AUTHOR CONTRIBUTIONS

William D. Figg, Jr.: Conceptualization; methodology; software; data curation; investigation; validation; formal analysis; visualization; writing – original draft; writing – review and editing. **Giorgia Fiorini:** Methodology; software; data curation; investigation; validation; formal analysis; visualization; writing – original draft; writing – review and editing. **Rasheduzzaman Chowdhury:** Conceptualization; methodology; investigation; validation; writing – review and editing. **Yu Nakashima:** Software; investigation; validation; writing – review and editing. **Anthony Tumber:** Methodology; software; investigation; validation. **Michael A. McDonough:** Conceptualization; methodology; software; investigation; validation; formal analysis. **Christopher J. Schofield:** Conceptualization; methodology; investigation; validation; formal analysis; supervision; funding acquisition; visualization; project administration; resources; writing – original draft; writing – review and editing.

ACKNOWLEDGMENTS

The authors thank our funding bodies the Wellcome Trust (091857/7/10/7), the Biotechnology and Biological Sciences Research Council (BB/L000121/1, BB/J001694/2, and BB/R013829/1) the Cancer Research UK (C8717/A18245) and a Newton Abraham studentship (to GF) for support of this work. The authors thank Diamond Light Source for the allocated beamtime (proposal-visit: MX-18069-63 and MX-18069-86), and the staff of the I24 beamline for assistance with crystal screening and data collection.

CONFLICT OF INTEREST STATEMENT

The authors declare no conflicts of interest.

DATA AVAILABILITY STATEMENT

Coordinates and structure factors for PHD2.HIF2 α -CODD complex structures were deposited in the RCSB Protein Data bank as: PHD2₁₈₁₋₄₀₇.Mn.NOg.HIF2 α ₅₂₃₋₅₄₂-CODD, PDB: 7Q5V and PHD2₁₈₁₋₄₀₇.Mn.2OG.HIF2 α ₅₂₃₋₅₄₂-CODD, PDB: 7Q5X. AlphaFold models and HIF α sequences were accessed using UniProt: Q96KS0-PHD1, Q9H6Z9-PHD3, Q16665-HIF1 α , Q99814-HIF2 α , and Q9Y2N7-HIF3 α .

ORCID

William D. Figg, Jr.  <https://orcid.org/0000-0002-5875-2606>

Giorgia Fiorini  <https://orcid.org/0000-0003-3885-4629>

Rasheduzzaman Chowdhury  <https://orcid.org/0000-0002-8058-6149>

Yu Nakashima  <https://orcid.org/0000-0001-7788-8333>

Anthony Tumber  <https://orcid.org/0000-0003-1958-8353>

Michael A. McDonough  <https://orcid.org/0000-0003-4664-6942>

Christopher J. Schofield  <https://orcid.org/0000-0002-0290-6565>

REFERENCES

1. Semenza GL. Hypoxia-inducible factor 1: master regulator of O₂ homeostasis. *Curr Opin Genet Dev.* 1998;8(5):588-594.
2. Kaelin WG, Ratcliffe PJ. Oxygen sensing by metazoans: the central role of the HIF hydroxylase pathway. *Mol Cell.* 2008;30(4):393-402.
3. Schofield CJ, Ratcliffe PJ. Oxygen sensing by HIF hydroxylases. *Nat Rev Mol Cell Biol.* 2004;5(5):343-354.
4. Chowdhury R, Hardy A, Schofield CJ. The human oxygen sensing machinery and its manipulation. *Chem Soc Rev.* 2008;37(7):1308-1319.
5. Maxwell PH, Wlesener MS, Chang GW, et al. The tumour suppressor protein VHL targets hypoxia-inducible factors for oxygen-dependent proteolysis. *Nature.* 1999;399(6733):271-275.
6. Stebbins CE, Kaelin WG, Pavletich NP. Structure of the VHL-elonginC-elonginB complex: implications for VHL tumor suppressor function. *Science.* 1999;284(5413):455-461.
7. Ivan M, Kondo K, Yang H, et al. HIF α targeted for VHL-mediated destruction by proline hydroxylation: implications for O₂ sensing. *Science.* 2001;292(5516):464-468.
8. Lando D, Peet DJ, Whelan DA, Gorman JJ, Whitelaw ML. Asparagine hydroxylation of the HIF transactivation domain: a hypoxic switch. *Science.* 2002;295(5556):858-861.
9. Chan MC, Ilott NE, Schödel J, et al. Tuning the transcriptional response to hypoxia by inhibiting hypoxia-inducible factor (HIF) prolyl and asparaginyl hydroxylases. *J Biol Chem.* 2016;291(39):20661-20673.
10. Elkins JM, Hewitson KS, McNeill LA, et al. Structure of factor-inhibiting hypoxia-inducible factor (HIF) reveals mechanism of oxidative modification of HIF-1 α . *J Biol Chem.* 2003;278(3):1802-1806.
11. Chowdhury R, McDonough MA, Mecinović J, et al. Structural basis for binding of hypoxia-inducible factor to the oxygen-sensing prolyl hydroxylases. *Structure.* 2009;17(7):981-989.
12. Epstein ACR, Gleadle JM, McNeill LA, et al. *C. elegans* EGL-9 and mammalian homologs define a family of dioxygenases that regulate HIF by prolyl hydroxylation. *Cell.* 2001;107(1):43-54.
13. Bruick RK, McKnight SL. A conserved family of prolyl-4-hydroxylases that modify HIF. *Science.* 2001;294(5545):1337-1340.
14. Islam MS, Leissing TM, Chowdhury R, Hopkinson RJ, Schofield CJ. 2-Oxoglutarate-dependent oxygenases. *Annu Rev Biochem.* 2018; 87(1):585-620.
15. Hewitson KS, McNeill LA, Riordan MV, et al. Hypoxia-inducible factor (HIF) asparagine hydroxylase is identical to factor inhibiting HIF (FIH) and is related to the cupin structural family. *J Biol Chem.* 2002; 277(29):26351-26355.
16. Tsukada Y, Fang J, Erdjument-Bromage H, et al. Histone demethylation by a family of JmjC domain-containing proteins. *Nature.* 2006; 439(7078):811-816.
17. Klose RJ, Kallin EM, Zhang Y. JmjC-domain-containing proteins and histone demethylation. *Nat Rev Genet.* 2006;7(9):715-727.
18. Myllyharju DJ. Prolyl 4-hydroxylases, key enzymes in the synthesis of collagens and regulation of the response to hypoxia, and their roles as treatment targets. *Ann Med.* 2008;40(6):402-417.
19. Flashman E, Hoffart LM, Hamed RB, Bollinger JM, Krebs C, Schofield CJ. Evidence for the slow reaction of hypoxia-inducible factor prolyl hydroxylase 2 with oxygen. *FEBS J.* 2010;277(19):4089-4099.
20. Tarhonskaya H, Chowdhury R, Leung IKH, et al. Investigating the contribution of the active site environment to the slow reaction of hypoxia-inducible factor prolyl hydroxylase domain 2 with oxygen. *Biochem J.* 2014;463(3):363-372.
21. Tarhonskaya H, Hardy AP, Howe EA, et al. Kinetic investigations of the role of factor inhibiting hypoxia-inducible factor (FIH) as an oxygen sensor. *J Biol Chem.* 2015;290(32):19726-19742.
22. Hirsilä M, Koivunen P, Günzler V, Kivirikko KI, Myllyharju J. Characterization of the human prolyl 4-hydroxylases that modify the hypoxia-inducible factor. *J Biol Chem.* 2003;278(33):30772-30780.
23. McNeill LA, Hewitson KS, Claridge TD, Seibel JF, Horsfall LE, Schofield CJ. Hypoxia-inducible factor asparaginyl hydroxylase

- (FIH-1) catalyses hydroxylation at the β -carbon of asparagine-803. *Biochem J.* 2002;367(3):571-575.
24. Tian YM, Yeoh KK, Lee MK, et al. Differential sensitivity of hypoxia inducible factor hydroxylation sites to hypoxia and hydroxylase inhibitors. *J Biol Chem.* 2011;286(15):13041-13051.
25. Chan DA, Sutphin PD, Yen SE, Giaccia AJ. Coordinate regulation of the oxygen-dependent degradation domains of hypoxia-inducible factor 1 α . *Mol Cell Biol.* 2005;25(15):6415-6426.
26. Appelhoff RJ, Tian YM, Raval RR, et al. Differential function of the prolyl hydroxylases PHD1, PHD2, and PHD3 in the regulation of hypoxia-inducible factor. *J Biol Chem.* 2004;279(37):38458-38465.
27. Chowdhury R, Leung IKH, Tian YM, et al. Structural basis for oxygen degradation domain selectivity of the HIF prolyl hydroxylases. *Nat Commun.* 2016;7(1):12673.
28. Chowdhury R, Abboud MI, McAllister TE, et al. Use of cyclic peptides to induce crystallization: case study with prolyl hydroxylase domain 2. *Sci Rep.* 2020;10(1):21964.
29. Abboud MI, Chowdhury R, Leung IKH, et al. Studies on the substrate selectivity of the hypoxia-inducible factor prolyl hydroxylase 2 catalytic domain. *ChemBioChem.* 2018;19(21):2262-2267.
30. Figg WD Jr, McDonough MA, Chowdhury R, et al. Structural basis of prolyl hydroxylase domain inhibition by Molidustat. *ChemMedChem.* 2021;16(13):2082-2088.
31. Choueiri TK, Kaelin WG. Targeting the HIF2-VEGF axis in renal cell carcinoma. *Nat Med.* 2020;26(10):1519-1530.
32. Lee YS, Vortmeyer AO, Lubensky IA, et al. Coexpression of erythropoietin and erythropoietin receptor in Von Hippel-Lindau disease-associated renal cysts and renal cell carcinoma. *Clin Cancer Res.* 2005; 11(3):1059-1064.
33. Xu R, Wang K, Rizzi JP, et al. 3-[(1S,2S,3R)-2,3-Difluoro-1-hydroxy-7-methylsulfonylindan-4-yl]oxy-5-fluorobenzonitrile (PT2977), a hypoxia-inducible factor 2 α (HIF-2 α) inhibitor for the treatment of clear cell renal cell carcinoma. *J Med Chem.* 2019;62(15):6876-6893.
34. Ohh M, Taber CC, Ferens FG, Tarade D. Hypoxia-inducible factor underlies von Hippel-Lindau disease stigmata. *eLife.* 2022;11:e80774.
35. McAllister TE, Yeh TL, Abboud MI, et al. Non-competitive cyclic peptides for targeting enzyme-substrate complexes. *Chem Sci.* 2018; 9(20):4569-4578.
36. Clifton IJ, McDonough MA, Ehrismann D, Kershaw NJ, Granatino N, Schofield CJ. Structural studies on 2-oxoglutarate oxygenases and related double-stranded β -helix fold proteins. *J Inorg Biochem.* 2006; 100(4):644-669.
37. McDonough MA, Li V, Flashman E, et al. Cellular oxygen sensing: crystal structure of hypoxia-inducible factor prolyl hydroxylase (PHD2). *Proc Natl Acad Sci U S A.* 2006;103(26):9814-9819.
38. Anagianni S, Tuschl K. Genetic disorders of manganese metabolism. *Curr Neurol Neurosci Rep.* 2019;19(6):33.
39. Loenarz C, Mecinović J, Chowdhury R, McNeill LA, Flashman E, Schofield CJ. Evidence for a stereoelectronic effect in human oxygen sensing. *Angew Chem Int Ed Engl.* 2009;48(10):1784-1787.
40. Lippel K, Boleininger A, McDonough M, et al. Born to sense: biophysical analyses of the oxygen sensing prolyl hydroxylase from the simplest animal *Trichoplax adhaerens*. *Hypoxia.* 2018;6:57-71.
41. Scotti JS, Leung IKH, Ge W, et al. Human oxygen sensing may have origins in prokaryotic elongation factor Tu prolyl-hydroxylation. *Proc Natl Acad Sci U S A.* 2014;111(37):13331-13336.
42. Schnicker NJ, Dey M. *Bacillus anthracis* prolyl 4-hydroxylase modifies collagen-like substrates in asymmetric patterns. *J Biol Chem.* 2016; 291(25):13360-13374.
43. Domene C, Jorgensen C, Schofield CJ. Mechanism of molecular oxygen diffusion in a hypoxia-sensing prolyl hydroxylase using multiscale simulation. *J Am Chem Soc.* 2020;142(5):2253-2263.
44. Hon WC, Wilson MI, Harlos K, et al. Structural basis for the recognition of hydroxyproline in HIF-1 α by pVHL. *Nature.* 2002;417(6892): 975-978.
45. Holt-Martyn JP, Chowdhury R, Tumber A, et al. Structure-activity relationship and crystallographic studies on 4-hydroxypyrimidine HIF prolyl hydroxylase domain inhibitors. *ChemMedChem.* 2020;15(3): 270-273.
46. Rabe P, Kamps JJAG, Sutherlin KD, et al. X-ray free-electron laser studies reveal correlated motion during isopenicillin N synthase catalysis. *Sci Adv.* 2021;7(34):eabh0250.
47. Islam MS, Markoulides M, Chowdhury R, Schofield CJ. Structural analysis of the 2-oxoglutarate binding site of the circadian rhythm linked oxygenase JMJD5. *Sci Rep.* 2022;12(1):20680.
48. Yeh TL, Leissing TM, Abboud MI, et al. Molecular and cellular mechanisms of HIF prolyl hydroxylase inhibitors in clinical trials. *Chem Sci.* 2017;8(11):7651-7668.
49. Ramanan R, Chaturvedi SS, Lehnert N, Schofield CJ, Karabencheva-Christova TG, Christov CZ. Catalysis by the JmjC histone demethylase KDM4A integrates substrate dynamics correlated motions and molecular orbital control. *Chem Sci.* 2020;11(36):9950-9961.
50. Ramanan R, Waheed SO, Schofield CJ, Christov CZ. What is the catalytic mechanism of enzymatic histone N-methyl arginine demethylation and can it be influenced by an external electric field? *Chem Eur J.* 2021;27(46):11750.
51. Tarade D, Lee JE, Ohh M. Evolution of metazoan oxygen-sensing involved a conserved divergence of VHL affinity for HIF1 α and HIF2 α . *Nat Commun.* 2019;10(1):3293.
52. Chowdhury R, Abboud MI, Wiley J, Tumber A, Markolovic S, Schofield CJ. Conservation of the unusual dimeric JmjC fold of JMJD7 from *Drosophila melanogaster* to humans. *Sci Rep.* 2022;12(1): 6065.
53. Jumper J, Evans R, Pritzel A, et al. Highly accurate protein structure prediction with AlphaFold. *Nature.* 2021;596(7873):583-589.
54. Loenarz C, Coleman ML, Boleininger A, et al. The hypoxia-inducible transcription factor pathway regulates oxygen sensing in the simplest animal, *Trichoplax adhaerens*. *EMBO Rep.* 2011;12(1):63-70.
55. Rytönen KT, Williams TA, Renshaw GM, Primmer CR, Nikinmaa M. Molecular evolution of the metazoan PHD-HIF oxygen-sensing system. *Mol Biol Evol.* 2011;28(6):1913-1926.
56. Mohlin S, von Stedingk K, Pietras A, Pählman S. No reason to reconsider HIF-2 as an oncogene in neuroblastoma and other cancer forms. *Proc Natl Acad Sci U S A.* 2017;114(51):E10856-E10858.
57. Wu D, Potluri N, Lu J, Kim Y, Rastinejad F. Structural integration in hypoxia-inducible factors. *Nature.* 2015;524(7565):303-308.
58. Percy MJ, Furlow PW, Beer PA, Lappin TRJ, McMullin MF, Lee FS. A novel erythrocytosis-associated PHD2 mutation suggests the location of a HIF binding groove. *Blood.* 2007;110(6):2193-2196.
59. Furlow PW, Percy MJ, Sutherland S, et al. Erythrocytosis-associated HIF-2 α mutations demonstrate a critical role for residues C-terminal to the hydroxylacceptor proline. *J Biol Chem.* 2009;284(14):9050-9058.
60. Percy MJ, Furlow PW, Lucas GS, et al. A gain-of-function mutation in the HIF2A gene in familial erythrocytosis. *N Engl J Med.* 2008;358(2): 162-168.
61. Perrotta S, della Regione F. The HIF2A gene in familial erythrocytosis. *N Engl J Med.* 2008;358(18):1965-1967.
62. Gale DP, Harten SK, Reid CDL, Tuddenham EGD, Maxwell PH. Autosomal dominant erythrocytosis and pulmonary arterial hypertension associated with an activating HIF2 α mutation. *Blood.* 2008;112(3):919-921.
63. Martini M, Teofili L, Cenci T, et al. A novel heterozygous HIF2AM535I mutation reinforces the role of oxygen sensing pathway disturbances in the pathogenesis of familial erythrocytosis. *Haematologica.* 2008;93(7):1068-1071.
64. van Wijk R, Sutherland S, Van Wesel ACW, et al. Erythrocytosis associated with a novel missense mutation in the HIF2A gene. *Haematologica.* 2010;95(5):829-832.
65. Winter G, Waterman DG, Parkhurst JM, et al. DIALS: implementation and evaluation of a new integration package. *Acta Crystallogr D Struct Biol.* 2018;74(2):85-97.

66. Adams PD, Afonine PV, Bunkóczi G, et al. PHENIX: a comprehensive Python-based system for macromolecular structure solution. *Acta Crystallogr D Biol Crystallogr*. 2010;66(2):213-221.
67. McCoy AJ, Grosse-Kunstleve RW, Adams PD, Winn MD, Storoni LC, Read RJ. Phaser crystallographic software. *J Appl Cryst*. 2007;40(4):658-674.
68. Emsley P, Cowtan K. Coot: model-building tools for molecular graphics. *Acta Crystallogr D Biol Crystallogr*. 2004;60(Pt 12 Pt 1):2126-2132.
69. Winn MD, Ballard CC, Cowtan KD, et al. Overview of the CCP4 suite and current developments. *Acta Crystallogr D Biol Crystallogr*. 2011;67(4):235-242.
70. Afonine PV, Grosse-Kunstleve RW, Echols N, et al. Towards automated crystallographic structure refinement with phenix.refine. *Acta Crystallogr D Biol Crystallogr*. 2012;68(4):352-367.
71. Chen VB, Arendall WB, Headd JJ, et al. MolProbity: all-atom structure validation for macromolecular crystallography. *Acta Crystallogr D Biol Crystallogr*. 2010;66(1):12-21.
72. Young JY, Westbrook JD, Feng Z, et al. OneDep: unified wwPDB system for deposition, biocuration, and validation of macromolecular structures in the PDB archive. *Structure*. 2017;25(3):536-545.

SUPPORTING INFORMATION

Additional supporting information can be found online in the Supporting Information section at the end of this article.

How to cite this article: Figg WD Jr., Fiorini G, Chowdhury R, et al. Structural basis for binding of the renal carcinoma target hypoxia-inducible factor 2 α to prolyl hydroxylase domain 2. *Proteins*. 2023;91(11):1510-1524. doi:[10.1002/prot.26541](https://doi.org/10.1002/prot.26541)